THE ASTRONOMICAL JOURNAL VOLUME 109, NUMBER 4 APRIL 1995

NEAR-INFRARED IMAGES OF IC 348 AND THE LUMINOSITY FUNCTIONS OF YOUNG EMBEDDED STAR CLUSTERS

ELIZABETH A. LADA[1,2]

Department of Astronomy, University of Maryland, College Park, Maryland 20742

CHARLES J. LADA[2]

Harvard-Smithsonian Center for Astrophysics, 60 Garden Street, Cambridge, Massachusetts 02138

Received 1994 October 14; revised 1995 January 12

ABSTRACT

We present the results of a sensitive near-infrared (*JHK*) imaging survey of the young cluster IC 348 and a nearby control field. From comparison of the cluster and control field observations we estimate that 380 sources, the majority of the stars observed in the cluster field, are members of the cluster. The spatial density of these stars is found to be significantly larger than that typical of classical open clusters but comparable to that which characterizes young embedded clusters such as NGC 2024 and the Trapezium. Overall, we find the surface density distribution of stars in IC 348 to be centrally concentrated and to decrease inversely with distance from the inner ($r \approx 0.1$ pc) to the outer ($r \approx 1.0$ pc) regions of the cluster. In detail the stellar surface density distribution of this cluster exhibits significant structure. Roughly half the stars are contained within a central subcluster with a radius of 0.5 pc. Outside this half-mass radius, we identify eight small subclusters which contain 10–20 stars and have radii 0.1–0.2 pc in extent. We construct the K luminosity function (KLF) for IC 348 and find it to increase with magnitude in a nonlinear, power-law fashion in the range $8 \leqslant m_K \leqslant 11$ mag. The measured slope (0.40) of the power-law portion of the IC 348 KLF is very similar to the slopes (0.37–0.38) determined for the KLFs of four young embedded clusters in Orion. The IC 348 KLF departs from a power-law shape at $m_K > 11$ magnitudes, and appears to decrease at magnitudes ($m_K \approx 14$) near the completeness limit of the survey. We construct evolutionary models for the near-infrared luminosity functions of young ($\tau_{cl} \leqslant 10^7$ yr) star clusters containing pre-main-sequence stars. We find that the KLFs of very young synthetic clusters evolve in a systematic and predictable manner as the clusters age. For a fixed IMF, the shape of a cluster KLF depends primarily on the duration of the star formation (τ_{sf}) and the age (τ_{cl}) of the cluster. In general we find that the luminosity functions of young clusters broaden with age. For coeval models (i.e., $\tau_{sf} \ll \tau_{cl}$) the slopes of the power-law portion of the KLFs exhibit significant variation with time, while models with continuous star formation (i.e., $\tau_{sf} \approx \tau_{cl}$) maintain more or less constant slopes as they age. The observed similarity between the KLF slopes of numerous embedded clusters and those of the models suggests that uniform, continuous star formation may be characteristic of the star formation histories of many embedded clusters. From comparison of our models with our observations of IC 348 we conclude that star formation in IC 348 has been a continuous process over the last $5–7 \times 10^6$ yr and that the overall rate of star formation and the rate of star formation as a function of mass has been constant over the cluster lifetime. From a comparative analysis of published observations of the Trapezium cluster with our models and observations of IC 348, we find that the underlying mass function of both clusters is similar to the IMF for field stars down to the hydrogen burning limit with little evidence for a significant population of single, lower mass objects (brown dwarfs). In addition we also find that despite the similarities in their mass functions, stellar densities, and sizes, IC 348 and the Trapezium have been characterized by significantly different rates of star formation over their lifetimes. The rate of star formation in the younger Trapezium cluster has been a factor of 20 greater than that in IC 348. Finally, analysis of the JHK colors of the stars in IC 348 reveals that ~20% of the cluster sources are infrared excess sources. The size of the population of infrared excess sources coupled with the age of the cluster suggests a lifetime of $2–3 \times 10^6$ yr for the (protoplanetary) disk phase of early stellar evolution, consistent with previous estimates.

1. INTRODUCTION

A fundamental consequence of the theory of stellar evolution is that the life history of a star is almost entirely predetermined by its initial mass. Consequently, to understand the star formation history and the consequent luminosity evolution of an embedded population of young stars or of the galaxy itself requires a detailed knowledge of both the initial distribution of stellar masses at birth and how this quantity varies through space and time. Unfortunately, stellar evolution theory is not able to predict the Initial Mass Function (IMF) of stars. This quantity must be derived from observations. In a classic paper nearly 40 years ago, Salpeter (1955)

[1]Hubble Fellow.

[2]Visiting Astronomer, Kitt Peak National Observatory, part of the National Optical Astronomy Observatories, which is operated by the Association of Universities for Research in Astronomy, Inc., under contract with the National Science Foundation.

 0004-6256/95/109(4)/1682/15/$0.90

used the luminosity function of present day field stars in the solar neighborhood to derive the field star IMF. Assuming a constant star formation rate over the age of the galaxy and correcting the present day field star mass function for stellar evolution, he found that the IMF could be well represented by a simple power law, $\xi(\log m_*) \sim m_*^{-1.35}$, for stars with masses in the range between 1–10 $\mathcal{M}_\odot$. The derived sign and slope of the Salpeter IMF indicates that most stars which form in the galaxy are of low mass and moreover that most of the stellar mass in our galaxy is contained in such stars. Subsequent studies, particularly by Scalo (1978, 1986) extended knowledge of the field star IMF to subsolar masses and found that the IMF has a peak at about 0.2–0.3 $\mathcal{M}_\odot$ and therefore turns over and departs from the Salpeter power law well above the hydrogen burning limit.

The field star IMF, by itself, however, may not necessarily provide a strong constraint for star formation theory, since it is a globally averaged IMF, averaged over both the lifetime of the galaxy and over a specific volume of space (i.e., the solar neighborhood). Although it is often assumed that the IMF is universal in both time and space, this has never been demonstrated in a completely satisfactory way. However, in order to develop comprehensive theories for star formation and galactic evolution it is crucial to know whether the detailed form of the IMF is universal. Are there spatial and/or temporal variations in the initial conditions and other important astrophysical parameters that can alter the process of star formation and the form of the IMF? Or is star formation such a robust process that the outcome is always an IMF of the same form?

In principle, observations of large enough groups of young or newly forming stars in different parts of the galaxy should be able to provide fundamental constraints on these questions. The smallest spatial size scale over which a meaningful determination of a luminosity function can be made is that characteristic of an open cluster. Clusters are important laboratories for studying the initial luminosity function because they consist of statistically significant groups of stars who share the common heritage of forming from the same parental cloud at the same epoch in time. Historically observations of classical open clusters have suggested a common shape of the cluster mass function for stellar masses above 1 solar mass (e.g., Taff 1974) and recent observations of the nearby Pleaides and Hyades clusters argue for cluster mass functions similar to the field IMF for masses down to the hydrogen burning limit (Stauffer *et al.* 1989; Reid 1993). However, classical open clusters are sufficiently old that issues such as dynamical mass segregation and evaporation of low mass stars make determinations of their IMFs somewhat uncertain. Of even greater concern is the possibility that open clusters can lose a significant fraction of their members during the process of emergence from the molecular clouds in which they are formed (Lada *et al.* 1984).

During the past several years, near-infrared imaging studies of star forming regions have revealed the existence of a large number of extremely young embedded clusters containing ~ hundreds of young stars (Barsony *et al.* 1991; Hodapp and Rayner 1991; Lada *et al.* 1991a; Lada *et al.* 1991b; Eiora and Casali 1992; Carpenter *et al.* 1993; Lada *et al.* 1993; Strom *et al.* 1993a). Such embedded young clusters offer unique opportunities for investigation of the stellar initial mass function and its possible variation in space and time. These clusters are not old enough to have lost significant numbers of members due to stellar evolution or dynamical effects such as evaporation or violent relaxation, (e.g., Lada *et al.* 1984; Lada & Lada 1991). Mass segregation is also not as big a potential problem as in classical open clusters. Moreover, in these very young ($1–5\times10^6$ yr) clusters, low mass stars are brighter than at any other time in their pre-main-sequence evolution. Consequently, modern infrared array detectors on modest sized telescopes can readily detect stars at the hydrogen burning limit and thus completely sample the entire IMF of nearby ($D \leq 1$ kpc) embedded clusters. The high luminosities of very young low mass stars coupled with the extremely high stellar surface densities of embedded clusters make the issue of membership determination much less a concern than it is for open clusters. In addition, these clusters are rich enough to provide a statistically significant sampling of the stellar mass function at virtually all masses above the hydrogen burning limit. On the other hand, issues such as differential reddening and pre-main-sequence evolution can raise complications and require special attention in the interpretation of embedded cluster data.

In this paper, we report the results of a sensitive near-infrared imaging survey of the nearby cluster IC 348. IC 348 is a relatively dense young cluster located in the Perseus Molecular Cloud at a distance of ~320 pc. Optically, the cluster contains about 40 stars, the brightest being the B5 V star BD+31°643, which is associated with a well-known reflection nebula. Studies of the optical reflection nebulosity (Witt & Schild 1986) and the molecular gas in the region (Kutner *et al.* 1980; Bachiller *et al.* 1987) suggest that the cluster is still embedded in its parental molecular gas and dust. Consequently, a significant portion of its membership may have escaped detection in existing optical studies. The idea that the cluster is young is supported by the detection of 16 Hα emission line objects (Herbig 1954) and a number of embedded infrared sources (Strom, *et al.* 1974). The age of the IC 348 cluster has been estimated to be roughly 5–20 million years (Strom *et al.* 1974). We obtained near-infrared observations of the cluster to make a more complete census of its membership, determine the nature of its embedded members, and construct the infrared luminosity function of the cluster. To investigate the nature of the underlying mass function we calculate models which predict the evolution of the luminosity function of a cluster of pre-main-sequence stars. We compare these models with observations of IC 348 and the Trapezium cluster to place constraints on the star formation histories of these clusters and on the nature of the underlying stellar mass functions. In the following sections (2 and 3), we present the observations and analysis of our near-infrared imaging data for the IC 348 cluster. The general properties of the cluster derived from these observations are discussed in Sec. 4. In Sec. 5 we present our model calculations and their comparison to the observations. In Sec. 6 we summarize our results.

2. OBSERVATIONS AND DATA REDUCTION

The near-infrared imaging data of the young cluster IC 348 were obtained using the National Optical Astronomy Observatory (NOAO) Simultaneous Quad Infrared Imaging Device (SQIID) on the Kitt Peak National Observatory (KPNO) 1.3 m telescope in 1991 September. SQIID is equipped with four 256×256 platinum silicide (PtSi) focal plane arrays. Dichroic mirrors were used to allow simultaneous observations at four infrared wavelength bands: J(1.2 μm), H(1.6 μm), K (2.2 μm), and L (3.4 μm). For this project, we obtained data only in the J, H, and K bands. The optics were configured to provide a field of view of approximately 5.'5×5.'5 and a resolution of 1.''36 per pixel at K band.

Twenty-four SQIID fields were observed toward the IC 348 cluster, covering an area of ~385 square arcmin. These fields were arranged in approximately a 5×5 mosaic centered on LkHα 90 (R.A.=$3^h41^m13^s.2$, Dec.=32° 00′ 52″). The fields were spatially overlapped by ~1.'5 in both right ascension and declination, allowing for both the accurate positional placement of the mosaicked fields and redundancy of our photometric measurements of sources located in the overlapped regions. Twelve control fields were also observed in order to account for the distribution of foreground/background field stars. These control fields were located off the cluster and were determined to be free of any significant molecular material by examination of CO surveys in this region (Bachiller & Cernicharo 1986) and the Palomar Sky Survey Prints. Specifically six of these off fields were observed ~1° north of the cluster center in a 2×3 mosaic and the other six were observed ~1° east of the cluster center in a 3×2 mosaic. The off field mosaics were not overlapped and therefore the total area observed off the cluster equals ~365 square arcmin. The integration time in each filter, for observations both on and off IC 348, was 3 min. We estimate the 5σ detection limits of our observations to be ~16.5, 15.5, and 14.5 mag at J, H, and K, respectively. Each cluster field was observed twice, with a 15″ offset or dither between observations.

The data were reduced using standard Image Reduction and Analysis Facility (IRAF) routines. First, a comparison sky frame was subtracted from each data frame. The sky frames were constructed from the filtered average of three nebulosity-free data frames, which were usually observed immediately before and after the target observation. The sky-subtracted frames were then divided by a flat field frame. Flat fields were obtained for each night and near-infrared color by median filtering ~65–100 data frames from that night's observations. The resulting median filtered images were then dark-subtracted and normalized to produce the flat fields. The two dithered observations of each cluster ("on") field were combined using IRAF to produce images with an effective integration time, in each filter, equal to 6 min. The 5σ detection limits for the combined images are 17, 16, and 15 mag at J, H, and K. Finally, the J and H images for each field, on and off IC 348, were registered to the positional grid of the corresponding K-band image using IRAF programs written by M. Merrill for SQIID reduction. The relative pointing offsets of these three channels were determined by observations of globular clusters (Merrill 1992).

3. ANALYSIS

3.1 Source Extraction and Photometry

Sources were identified and counted using the DAOFIND routine (Stetson 1987) within the IRAF package. DAOFIND was run on each image separately, using a full width at half-maximum (FWHM) of the point spread function between 1.7 to 2.0 pixels and a single pixel finding threshold equal to four times the mean noise of each image. The results and images were carefully inspected. The DAOFIND coordinate files were edited to remove bad pixels and objects misidentified as stars and to append stellar sources that were not originally extracted by the finding routine.

Aperture photometry was performed for all sources on each image using the IRAF routine APPHOT. Fluxes were measured in an aperture, 3 pixels (3.''9) in radius, centered on the source. This aperture size corresponds to ~3 times the FWHM of the typical point spread function for our SQIID data. Sky values around each source were determined from the mode of pixel intensities in an annulus having an inner radius of 10 pixels and an outer radius of 20 pixels. Using an aperture with a three pixel radius ensured that the flux from ~90% of the sources was not contaminated by the flux from nearby stars. However, this aperture was too small to contain all the flux from a source. Therefore, in order to account for the missing flux, multiaperture photometry was performed for each image on all bright (m_J, m_H, m_K<12), isolated sources. For these sources, the flux obtained in the 3 pixel radius aperture was compared with flux measured in a larger, 8 pixel radius aperture, and the fraction of the total source flux falling within the 3 pixel radius aperture was then determined. Typically, the 3 pixel radius aperture was found to contain approximately 93% of the total source flux. The instrumental magnitudes for all SQIID sources were corrected to account for the missing flux.

Photometric calibration for our data was accomplished using the list of Elias standard sources. Standards were observed on the same nights and through similar airmasses as were observations of cluster on and off images. Since the SQIID system is close to the Johnson system (e.g., Lada *et al.* 1993) we elected to use the SQIID camera filters and arrays as our standard system and to use in-band observations of the standards to establish the filter zero points independently. Since the standards were observed at nearly the same airmasses and infrared extinctions are very small (0.1–0.2 mag per airmass), our reported magnitudes and colors are likely not in error by much more than their photometric uncertainties determined by APPHOT. On 1991 September 25, the standard star HD 203856 was observed at nine different locations on the SQIID arrays to estimate the sensitivity variations across the chips. All J, H, and K measurements of the standards during our observing sessions were consistent to within 5%.

A number of cluster (on) sources were observed at least twice due to spatial overlapping of the image grids. These sources allow us to check the consistency of our photometry measurements. Specifically, 245 sources were observed twice

at J, 270 at H, and 208 at K. The photometry of the duplicate pairs agree on average to within ~6% for sources having $m_J<16$, $m_H<15$, $m_K<14$, and to within 10% for sources having $m_J<17$, $m_H<16$, and $m_K<15$.

3.2 Completeness Limits

In order to estimate the completeness limits of this survey, we compared the number of stars identified, as a function of magnitude, on pairs of dithered images. DAOFIND and PHOT were run on the overlapping regions of 15 pairs of dithered cluster field images, using the same criteria described above. The apparent magnitude distribution of stars that were identified and matched across the dithered pairs of images was compared to the magnitude distribution of stars that were found in only one of the image pairs. From this comparison, we estimate that the identification of sources in the individual image frames is ~90% complete to $m_J=15.5$, $m_H=14.5$, and $m_K=13.5$. These completeness limits are extended another 0.75 mag, for the pairs of dithered cluster "on" images that were registered and combined.

3.3 Positions

Absolute α and δ positions were determined for each individual cluster source identified by our survey. A centering algorithm in APPHOT was used to obtain center positions for the sources in pixels. The IC 348 cluster fields contained many stars in the overlapped regions. Duplicate stars on adjacent frames were used to register the relative pixel positions of the individuals SQIID frames onto a single positional grid centered on LkHα90. The plate scale of the grid was determined by measuring the grid locations of several bright LkHα stars whose positions were already well known. Pixel positions were converted to α and δ offsets using the K-band array plate scale of 1.″36 per pixel.

4. RESULTS

As a result of our SQIID survey toward IC 348, we detected a total of 669 sources at J-band ($m_J<17$), 657 sources at H ($m_H<16$) and 552 sources at K ($m_K<15$). Figure 1 (Plate 65) presents our K-band image of IC 348. This image is a mosaic of 24 individual SQIID frames. The bright star located in the upper central portion of the image is o Per. A clustering of infrared sources is clearly seen to the south of o Per. The brightest star seen toward the cluster center is BD +31°643. We note that o Per is saturated in each of our J, H, and K images. For this reason and since this star is also thought to lie beyond IC 348, we have excluded it in our photometric and color analysis.

Near-infrared surveys of molecular clouds have shown that the contribution by foreground/background field stars to these surveys can be significant (Straw & Hyland 1989; Lada *et al.* 1991). Therefore, before any conclusions about the near-infrared observations of IC 348 can be made, it is necessary to account for field star contamination. Observations of control or off fields were used to determine the properties of the field star population in the vicinity of the IC 348 cluster. In the nearly equal sized off-field region, 466 sources at J-band ($m_J<17$), 373 sources at H ($m_H<16$) and 215 sources at K ($m_K<15$) were identified. To estimate the size of the field star population contained in the IC 348 field, the control field stars were artificially extincted by 1.29 mag at J, 0.80 mag at H, and 0.50 mag at K to account for the extinction toward IC 348 due to the associated molecular cloud. The amount of extinction was estimated by direct comparison of the average $H-K$ colors of the cluster and control field stars as discussed below (see Sec. *4.2*). Comparing the cluster field observations with those of the extincted control fields for magnitudes brighter than our completeness limits, we find an excess of 377 stars at J-band ($m_J<16$), 366 at H-band ($m_H<15$) and 345 at K-band ($m_K<14$) toward IC 348. These are likely underestimates to the true sizes of the cluster population, since, as we discuss later, the amount of extinction we derive probably underestimates the actual extinction to the background stars.

4.1 Spatial Distribution of Sources & Stellar Densities

The spatial distribution of near-infrared sources in our JHK band images (e.g., Fig. 1) is nonuniform, with a large fraction of the sources being concentrated in one large central clustering to the south of o Per. Moreover, the spatial distribution of sources outside this central concentration also shows evidence of significant structure and subclustering. In order to obtain a more quantitative estimate of the stellar surface density and its variation across the cluster, we have constructed a star count map of our K-band observations of the cluster. The star counts were obtained by subdividing the region of our IC 348 observations into a rectilinear grid of overlapping squares and counting the number of stars in each square. The squares were 1.5′×1.5′ in size and were separated by 0.75′, the Nyquist spatial sampling interval. The resulting contour map of the stellar surface density is shown in Fig. 2. The lowest contour level corresponds to a surface density roughly equal to the estimated background/foreground field star density and the spacings between contours are multiples of this value. The lowest solid line contour represents a surface density of about three times the field star density. Much structure is seen in this figure and we have identified nine significant subclusterings of stars at the 5 sigma level above the background/foreground field star distribution. The locations and observed properties of these subclusters are listed in Table 1. The observed properties (i.e., number of sources, size, and stellar density) of the individual subclusters (IC 348a-i) were determined for the areas contained within the 3 sigma level contour of each stellar group. The number of sources in each group was corrected for background/foreground field stars. The effective sizes of the subclusterings were estimated assuming the groups were spheres located at a distance of 320 pc. Approximately 50% of the sources associated with IC 348 are found within the main subcluster (IC 348a) located at the offset position of (2.8,−1). This sub-clustering contains 160 sources within a radius of ~0.5 pc. The eight subgroupings of stars (IC 348b-i) surrounding IC 348a are significantly smaller. They contain ~5–20 sources and have radii ranging from 0.1–0.2 pc.

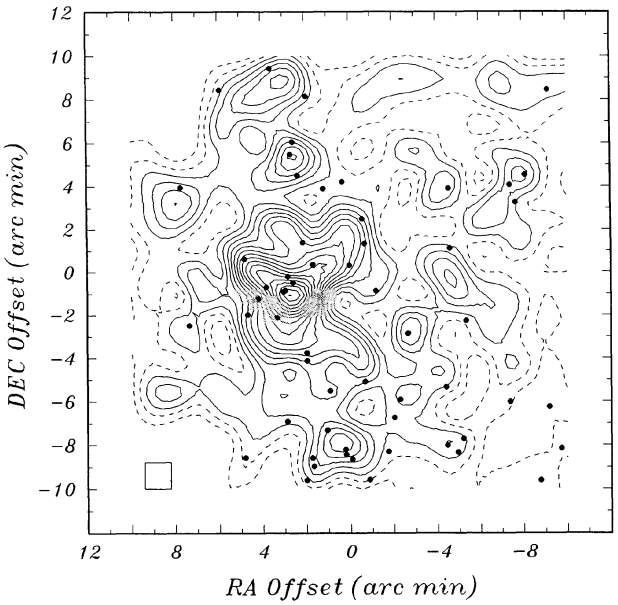

FIG. 2. Contour map of the stellar surface density distribution for the IC 348 cluster. The (0,0) position corresponds to α=3^h 41^m 13^s.2, δ=32° 00′ 52″. The lowest contour level corresponds to the estimated surface density of background/foreground field stars in this region and subsequent levels are multiples of this value. The lowest solid contour level represents a surface density equal to three times the estimated field star density. The filled circles show the locations of the sources having *JHK* colors suggestive of near-infrared excess emission.

The overall stellar surface density of the IC 348 cluster, determined for the entire area surveyed, ($r \approx 1.0$ pc) is ~105 stars pc^{-2}. Progressively higher densities are found if progressively smaller spatial scales are considered. The surface density of the sources contained within the 3 sigma boundary ($r \approx 0.47$ pc) of the main cluster (IC 348a) is ~230 stars pc^{-2}. Within the innermost region of this main subcluster, a 0.1 pc radius encompasses ~30 stars, giving a stellar density ~955 stars pc^{-2}. This indicates that the overall surface density distribution of stars is centrally concentrated and falls off roughly as r^{-1}, which is similar to the radial variation of surface density in the Trapezium cluster (McCaughrean & Stauffer 1994). The stellar surface density we derive for the inner 0.1 pc of IC 348a, although large, is comparable to the surface densities derived on similar spatial scales for the Trapezium (3100 stars pc^{-2}; McCaughrean & Stauffer 1994) and NGC 2024 (1600 stars pc^{-2}; Lada *et al.* 1991b), two young embedded clusters in Orion.

TABLE 1. Properties of subclusters.

Sub-Cluster	R. A. Offset[1] arcmin	Dec. Offset[1] arcmin	# of Stars $m_K < 14$	Radius pc	Stellar Density #/pc^{-2}
a	2.8	-1.0	160	0.47	230
b	0.5	-8.0	12	0.16	150
c	8.3	3.0	5	0.15	71
d	3.2	8.8	15	0.21	100
e	2.6	5.4	18	0.18	180
f	-7.8	4.5	7	0.13	140
g	-6.6	2.9	7	0.11	175
h	-4.4	-0.3	10	0.20	83
i	-2.8	-2.8	8	0.10	266
a: core	2.8	-1.0	30	0.10	955

[1] (0,0): R.A. = 3^h 41^m 13^s.2, Dec. = 32° 00′ 52″

The implied volume mass density for the IC 348 cluster is considerably in excess of that typical of an optically visible open cluster. For example, within its half-mass radius, the mass density of the Pleaides cluster is 2 $\mathcal{M}_\odot$ pc^{-3}. The corresponding value for the half-mass radius (0.47 pc) stellar mass density of IC 348 is 220 $\mathcal{M}_\odot$ pc^{-3} (assuming spherical geometry and an average stellar mass of 0.6 $\mathcal{M}_\odot$ for the stars in the cluster). The large disparity between the stellar densities of young embedded clusters, such as IC 348, NGC 2024 and the Trapezium, and classical open clusters, such as the Pleaides, is entirely consistent with predictions of models for the dynamical evolution of young clusters which form in molecular clouds with low star formation efficiencies (e.g., Lada *et al.* 1984). In this context, it is interesting to note that, if spread uniformly over volume, the stellar mass density of IC 348a would correspond to a molecular hydrogen volume density of roughly 5×10^3 cm^{-3}. This is a factor 2–4 lower than typical of dense molecular cloud cores and would be roughly consistent with a star formation efficiency of 25%–50% for this cluster.

On the 0.1 pc scale of their central regions, the implied stellar mass and equivalent molecular cloud densities of embedded clusters such as IC 348, NGC 2024, and the Trapezium are even larger. Correcting for projection effects according to the prescription of McCaughrean & Stauffer (1994), we estimate these values to be $2.5–8.2\times10^3$ $\mathcal{M}_\odot$ pc^{-3} and $5–16\times10^4$ cm^{-3}, respectively (for these three clusters). This latter range is within the range of molecular hydrogen densities measured on similar spatial scales in the most dense regions of massive cloud cores (e.g., Lada *et al.* 1995). This would seem to have important consequences for star formation theory and our understanding of protostars, especially if we consider that a 0.1 pc radius corresponds to the size scale expected for the protostellar envelope of a single star (Adams *et al.* 1987). This is also the characteristic size of a dense core in the Taurus molecular cloud which forms only one to at most a handful of stars. If these high stellar densities were characteristic of those at formation, then in the central regions of these clusters, the typical distance separating protostars would be relatively small (i.e., ≈6000 a.u.; McCaughrean & Stauffer 1994) suggesting that considerable interaction would be possible between protostellar objects as they and the cluster evolved. However, it is possible that the presently observed high stellar densities do not reflect the initial protostellar densities. The dynamical time scales (10^{4-5} yr) of such clusters are substantially less than their ages ($1–10\times10^6$ yr) indicating that significant dynamical evolution could have taken place since the clusters formed. In models for cluster formation in which the stars are formed with velocities smaller than the general velocity dispersion of the surrounding molecular gas, the stars can evolve to denser configurations than they start out with (Lada *et al.* 1984; Patel & Pudritz 1994).

The stellar surface densities for the smaller subclusters

(IC 348b-i) are also large, ranging from ~70–270 stars pc^{-2}. Even though the numbers of stars in these subclusterings are small, their stellar densities are typical of the embedded cluster as a whole and in addition are consistent with those expected due to the general r^{-1} falloff in overall cluster surface density. Consequently, these subclusters may be a result of the expected statistical fluctuations in the outwardly decreasing surface density distribution of the cluster as a whole. However, we note that these densities are significantly in excess of those (4–13 pc^{-2}) derived for the recently identified clusters in the Taurus cloud (Gomez *et al.* 1993). Although the Taurus groups contain similar numbers of stars, their estimated stellar densities are roughly an order of magnitude smaller than those of IC 348 b–i.

4.2 Color–Color Diagram

A large fraction of the near-infrared sources detected in our survey were detected in all three wavelength bands. Of the 552 sources detected at K (m_K<15) toward the IC 348 cluster, 500 of these were also detected at J and H. In addition, 162 background sources were detected at J, H, and K. The $J-H$ and $H-K$ colors were determined for all these sources for which the JHK photometric errors were ≤10%. The JHK color–color diagrams are plotted in Figs. 3(a) and 3(b) for the resulting 57 background and 342 cluster sources, respectively. In these figures, the locus of points corresponding to the unreddened main sequence is also plotted as a solid line and the locus of points corresponding to giant stars is plotted as a heavy dashed line. The two short dashed lines in each figure are drawn parallel to the reddening vector. The area between these lines corresponds to the reddening zone for normal stars. The crosses located on the reddening lines are separated by distances corresponding to 5 mag of visual extinction.

The color–color diagrams for the background sources and the cluster sources are noticeably different. Most of the stars in the control fields are located near the unreddened main-sequence line. The stars toward the cluster, however, are distributed over a large area of the color–color plot. The majority of cluster stars are located within the reddening bands but above the main-sequence line. This displacement of the cluster sources along the reddening vector is mainly due to extinction caused by the molecular cloud associated with the cluster. A large fraction of cluster stars are concentrated in a clump directly above the main-sequence line. Comparison of the location of this concentration of sources in the cluster color–color diagram with the distribution of stars in the off-field color–color diagram suggests a visual extinction of approximately 4.5 mag toward background field stars in the direction of the cluster. However, we also note that a significant number of stars in the cluster field are found spread along the reddening band beyond the main concentration of sources. This indicates that the extinction caused by the cloud is variable and can reach higher values. This, coupled with the fact that statistically most of the stars in the cluster field are cluster members and not background stars, suggests that our estimate of the extinction to the background stars is likely an underestimate and that the cluster stars themselves

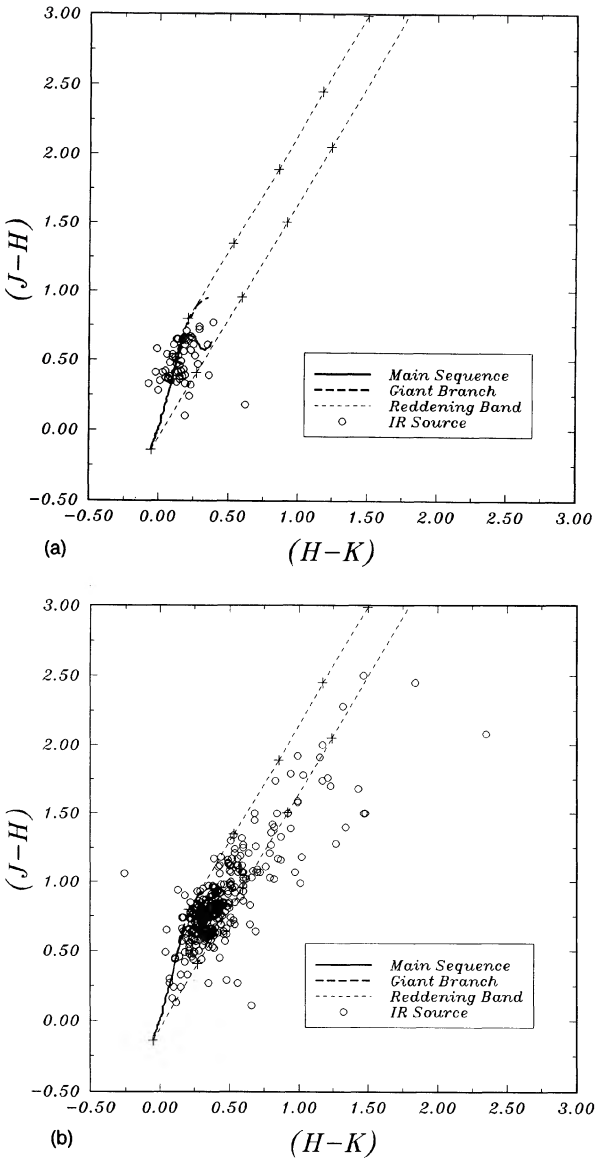

FIG. 3. The JHK color–color diagram for the IC 348 (a) control fields and (b) cluster. Only sources extracted from the observations with JHK photometric errors less than 10% are plotted. In addition, the solid line represents the locus of points occupied by unreddened main-sequence stars and the heavy dashed line the locus of positions of giant stars. The short dashed lines define the reddening band for normal stars and are parallel to the reddening vector in this diagram. Crosses are placed along these lines at intervals corresponding to five magnitudes of visual extinction.

are typically extincted by 4.5 visual magnitudes.

A small but significant number of cluster stars fall outside and to the right of the reddening lines. This region of the JHK color–color diagram is known as the infrared excess region (Lada & Adams 1992). A total of 58 sources or 17% of the sources that were detected at J, H, and K toward the cluster fall in this excess region. Correcting for field star contamination, we estimate that ~21% of the cluster members have colors suggestive of infrared excess emission.

The spatial distribution of near-infrared excess sources is presented in Fig. 2 in which the excess sources are shown as

filled circles. The NIR excess sources are found throughout the entire cluster region. Of the 58 excess sources, 19 (33%) are located in the main subcluster, while 39 (67%) are located outside this main group, either in the smaller subclusters or between subclusters. Furthermore, a higher fraction of sources located in the outer regions of the cluster (21%) exhibit excess emission, compared to the fraction in the main concentration (12%).

4.3 Luminosity Functions

The K-band luminosity function (KLF) for the stars observed toward the IC 348 cluster and the luminosity function for the stars in the off or control fields are presented in Fig. 4. The KLFs are displayed as histograms of the number of sources versus the apparent K magnitude, the bin size equaling 0.5 mag. As described above, the control field stars were each artificially extincted by 0.5 mag at K to approximately account for the extinction due to the associated molecular cloud. Comparison of the cluster and extincted control field luminosity functions shows that statistically, the majority of the stars detected toward IC 348 are cluster members. The field star contamination in the direction of IC 348 is minimal, except at the faintest magnitudes. For the extincted control-field KLF, the number of 2.2 μm sources increases as the K magnitude becomes fainter. At m_K=15.0, the extincted control-field KLF turns over. This turnover occurs beyond our estimated completeness limit (m_K=14.0) and is due to incompleteness in identifying faint sources. The shape of the KLF for stars observed toward the cluster is somewhat different. In this distribution, the number of 2.2 μm sources increases with increasing K magnitude until $m_K \sim 11.0$, after which the number of sources levels off. The observation that the number of sources toward the cluster remains roughly constant, suggests that the cluster luminosity function probably turns over at faint magnitudes.

Figure 4(b) shows the KLF resulting from the subtraction of the luminosity functions of the cluster and extincted control field, plotted as $\log N$ vs m_K. This differential KLF should represent the luminosity function of the cluster members. For magnitudes brighter than $m_K \sim 11.0$, the luminosity function can be fit by a power law. A linear, least-squares fit to the data between 6 and 11 mag gives a slope of 0.40 and is shown in Fig. 4(b). For magnitudes fainter than $m_K \sim 11.0$, the luminosity function deviates from this power law and flattens out. This flattening of the KLF occurs several magnitudes above our completeness limit. Finally, the KLF appears to fall off and turn over near the completeness limit.

Since 50% of the K-band sources associated with IC 348 are located in the main subcluster (a), the KLF for this subcluster was constructed and compared to the KLF for the entire cluster. The two KLFs were found to be nearly identical. Specifically, the main subcluster KLF can be described by a power law of slope $\alpha_K \sim 0.38$ out to $m_K \sim 11$ at which point it departs from a power law and flattens out.

The J-band luminosity function (JLF) for IC 348 was also constructed from our observations. The control field JLF was shifted to fainter magnitudes by 1.29 mag at J to account for extinction and subtracted from the cluster field JLF. The resulting differential JLF is similar in form to the corresponding KLF. The J luminosity function rises until a J magnitude $\sim$13 and then flattens out. The JLF turns over at $m_J \sim 15$ which is well above the completeness limit at J ($m_J \approx 16.0$). The slope of the JLF is somewhat shallower than the slope for the KLF. A linear least-squares fit to the data between m_J=6 and 13 indicates that the JLF is well described by a single slope of 0.32 in this range.

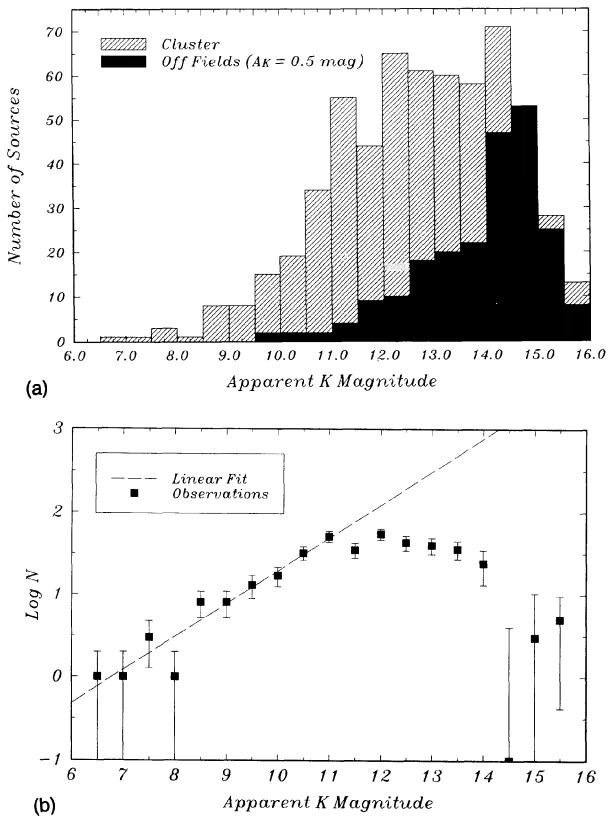

FIG. 4. (a) The K luminosity function for all sources observed toward IC 348 is plotted as a histogram of number vs the apparent K magnitude. The bin sizes correspond to 0.5 mag. For comparison, the corresponding K luminosity function for the control fields observed off the cluster is also plotted. The off-field KLF was shifted by 0.5 mag to account for extinction. (b) The differential K luminosity function for IC 348. This luminosity function was constructed by differencing the K luminosity functions of the cluster and extincted control fields. The resulting KLF is plotted as $\log N$ vs apparent K magnitude. This KLF should represent the K luminosity function of the cluster members. The dashed line shows the results of a least-squares analysis for m_K<11.

5. DISCUSSION

5.1 Cluster Luminosity Functions

The J and K luminosity functions of the IC 348 cluster exhibit two distinct features. First, both luminosity functions appear to be power law in form for the brightest stars and second, their shape departs from a power law at the faintest magnitudes. These characteristics are evident in the K luminosity functions of several other young embedded or par-

tially embedded clusters (Lada *et al.* 1991; Lada *et al.* 1993) and also in the initial mass function (IMF) for field stars (Scalo 1986).

Comparison of the K luminosity functions for young clusters reveal that they have remarkably similar slopes. For example, the slope of the IC 348 KLF (0.40) is nearly identical to the slopes of the KLFs obtained for young clusters in the Orion molecular clouds. Lada *et al.* (1991) derived slopes ranging from 0.37 to 0.38 for the three rich clusters, NGC 2024, NGC 2068, and NGC 2071, in the Orion B (L1630) molecular cloud. The KLF for the Trapezium cluster (Zinnecker *et al.* 1993), also has a slope equal to 0.38. In addition, the IC 348 and Orion cluster KLFs are similar to, although somewhat steeper than the slope (0.32) derived for the KLF of NGC 2264 (Lada *et al.* 1993).

The second characteristic of the IC 348 luminosity function, the flattening and turnover of the luminosity function at faint magnitudes is also seen in the KLFs of the young clusters NGC 2264 and the Trapezium, for which sufficiently sensitive near-infrared observations have been obtained. The KLF for IC 348 starts to flatten out at $m_K \sim 11.5$. For NGC 2264, the KLF departs from the power-law fit at a K magnitude of approximately 13.0 (Lada *et al.* 1993) whereas for the Trapezium this occurs at a K magnitude of ~ 11 (Zinnecker *et al.* 1993) The KLFs for both NGC 2264 and IC 348 appear to turn over near K magnitudes of 14–14.5. These magnitudes are near the completeness limits for both surveys and therefore it is difficult to assess the significance of the observed turnovers. However, a much clearer indication of a turnover in the KLF is seen in the Trapezium cluster. For this cluster, the K luminosity function starts to decrease at K magnitudes fainter than $m_K \sim 12$. Furthermore, Zinnecker *et al.* (1993) did not detect *any* K-band sources between $m_K = 14$ to 15, the latter being the completeness limit of their survey.

In principle, the luminosity functions of young clusters should be related to their initial mass function. Consequently, investigations and comparisons of the K luminosity functions for young embedded and partially embedded clusters should provide constraints on the shape and universality of the IMF. The near-infrared luminosity functions for the sample of young clusters discussed above are surprisingly similar. In particular the slopes of the KLFs for these clusters appear to be quite robust, with most of the clusters having slopes around 0.38. It is interesting to note that these slopes are much steeper than that expected for a population of ZAMS stars whose distribution of masses is given by the field star IMF (e.g., Lada *et al.* 1991; Lada *et al.* 1993). Lada (1991) suggested that the relatively steep slopes of the KLFs for the L1630 clusters could be due to evolution, i.e., that most stars, especially the low mass ones, are still in the pre-main-sequence (PMS) phase of their evolution. Low mass PMS stars have much higher luminosities for their mass than main-sequence stars, whereas higher mass PMS stars will have luminosities closer to their main-sequence equivalents. This would create an excess of intermediate luminosity sources relative to high luminosity sources in a young cluster and hence steepen the slope of the KLF in the high-to-intermediate luminosity range. Unfortunately, it is not straightforward to test this hypothesis since there is no unique mass-to-luminosity relation for PMS objects. Recently, Lada (1994) attempted to predict the slope of the KLF for a cluster of pre-main-sequence stars by using a mass to K luminosity relation derived for 1×10^6 yr old pre-main-sequence stars in the Taurus clouds (Simon *et al.* 1992) and adopting a power-law slope for the mass function which is appropriate for low mass stars (Scalo 1978). The predicted slope of the KLF was 0.38, which is in good agreement with the observed KLFs for IC 348, the Orion clusters, and NGC 2264 and provides strong support for the hypothesis that the steep slopes of the observed KLFs are primarily a result of a large population of pre-main-sequence stars within these clusters.

The idea that the KLFs for the Orion clusters are consistent with the field star IMF and a mass–luminosity relation for 10^6 yr old PMS stars is not too surprising since these clusters are thought to be very young and have ages on the order of a million years (e.g., Trapezium; Prosser *et al.* 1994). However, both IC 348 and NGC 2264 are thought to be considerably older. The age of IC 348 has been estimated to be $5–20 \times 10^6$ yr (Strom *et al.* 1974) and the age of NGC 2264 has been estimated to be roughly 5×10^6 yr. Therefore, it is curious that the KLF slopes for these two clusters are similar to those of much younger clusters, especially since one might expect the mass–luminosity relation to change with time as the PMS population evolves and the KLF slopes to decrease toward the shallower value (0.26) representative of ZAMS stars. Why then are the slopes of the K luminosity functions for these young clusters of differing age so similar? To address this question requires an improved, time-dependent model for the KLF of a young cluster of pre-main-sequence stars. In particular, the pre-main-sequence mass–luminosity relation must be determined for a range of cluster ages and a more realistic mass spectrum must be adopted.

Recently, Zinnecker *et al.* (1993) and Fletcher & Stahler (1994a, b) have used computers to model the luminosity functions of very young clusters with realistic stellar mass functions and appropriate mass–luminosity relations derived from theoretical calculations of pre-main-sequence evolution. Fletcher and Stahler have derived bolometric luminosity functions for a suite of model clusters ranging in age from 10^4 to 10^7 yr and assuming a continuous star formation rate over the age of the cluster. However, because these models predict the bolometric luminosity functions of clusters they cannot be readily compared to the large database of existing monochromatic infrared observations. Nonetheless, these calculations were able to match reasonably well the bolometric luminosity function of the 10^6 yr old Rho Ophiuchi cluster. Zinnecker *et al.*, on the other hand, derived the monochromatic KLFs for a suite of synthetic clusters with ages between 10^5 and 2×10^6 yr. Unlike Fletcher and Stahler, Zinnecker *et al.* assumed coeval star formation in their calculations. Their models exhibit significant variations in the shape of the KLF as their clusters age and do not appear to be able to explain the lack of such variation in the data. However, their models are calculated for the very early stages ($\tau_{cl} \leq 2 \times 10^6$ yr) of cluster evolution and are clearly not

appropriate for objects such as IC 348 and NGC 2264. In the next section of this paper we describe new model calculations we have undertaken to predict the KLFs of young embedded clusters with ages between 10^6 and 10^7 yr. We have used a realistic IMF and recent numerical calculations of pre-main-sequence stellar evolution to construct models for clusters characterized by coeval and continuous star formation. The primary objective of this exercise was to directly compare synthetic KLFs with observations to place constraints on the star formation history and underlying IMF of IC 348 and other young embedded clusters as well.

5.2 Model Luminosity Functions

5.2.1 Underlying stellar mass function

The K luminosity function, dN/dK, of a very young cluster, is the product of the mass to K luminosity relation for PMS stars and the underlying stellar mass function, i.e.,

$$\frac{dN}{dK}=\frac{dN}{d\ \log M}\times\frac{d\ \log M}{dK}\ .$$

Therefore to model embedded cluster KLFs, requires a knowledge of both the IMF and the luminosity evolution of PMS stars. For our models we assumed a Miller–Scalo IMF,

$$\frac{dN}{d\ \log M}=C_0\ \exp[-C_1(\log M-C_2)^2],$$

where $C_0=106.0$, $C_1=1.09$, and $C_2=-1.02$ ((Miller & Scalo 1979). In order to produce a synthetic luminosity function to compare with observations, this mass function was numerically integrated over the individual intervals of mass, which for a given mass–luminosity relation, correspond to the appropriate half-magnitude bins in the K luminosity function. The synthetic KLFs were constructed for a population of stars whose masses were in the range between 0.1 to 20 $\mathcal{M}_\odot$. For simplicity we assumed that all the pre-main-sequence stars in the cluster were post-birthline objects. That is, we did not include protostars in our calculations. The validity of this assumption appears supported by Fletcher & Stahler's model (1994a, b) which suggest that protostars are a small fraction of the stellar population in clusters whose ages are in excess of 10^6 yr. The mass versus m_K relations for the synthetic stars were obtained for PMS stars using the recently published PMS tracks of D'Antona & Mazzitelli (1994) for stars having $M\leqslant 2.5\ \mathcal{M}_\odot$. The tracks used in our models were derived assuming Alexander opacities and the Canuto and Mazzitelli convection model. The PMS tracks provided us with a $L/L_\odot$ and $T_{\rm eff}$ for a star of given mass and age. For each star, the $T_{\rm eff}$ was used to obtain a spectral type and the spectral type was used in turn to obtain a bolometric correction at K. For statistical purposes, we modeled young clusters containing 1000 stellar members. We made no attempt to account for infrared excess emission and essentially assumed that our pre-main-sequence stars were diskless. The effects of infrared excess on the derived KLFs are to a large extent mitigated by the fact that we bin the model luminosity functions in relatively wide, 0.5 mag, bins similar to the observations. In IC 348 80% of the stars do not exhibit detectable excess emission in the JHK color–color diagram. This indicates that the amount of infrared excess in the K band is less than about 0.1 mag. The remaining 20% of the stars do have detectable infrared excess, which we estimate amounts to typically about 0.3 mag. This is similar to the magnitude of infrared excess for excess sources in other regions, but still smaller than the size of the bins used for the observed and model luminosity functions. Thus we expect that the model luminosity functions would not be greatly altered even if a large fraction of its stars were infrared excess sources.

5.2.2 The effects of unresolved binary stars

We have made no attempt to adjust the models to account for the presence of unresolved binary stars. However, since roughly half of all stars are thought to be binary systems, it is of some interest to consider the effects that the presence of unresolved binary systems would have on both our synthetic KLFs and that of the IC 348 cluster. We note that at 320 pc, binaries with separations less than about 800 a.u. are unresolved by our observations of IC 348. Since nearly 90% of all binary stars in the field appear to have separations smaller than this (Duquennoy & Mayor 1991), the observed KLF of IC 348 probably does not represent a single star luminosity function. Indeed, we expect roughly 40% of the sources we observe in IC 348 to be unresolved binaries. There are two ways in which unresolved binary stars can potentially alter a stellar luminosity function.

First, the luminosities of unresolved binary systems are larger than those of a single star. Consequently, one expects the luminosity function of a cluster of binary stars to be shifted to higher luminosities than that of a cluster of only single stars. However, since the masses of companion stars are not correlated with the masses of primaries (e.g., Duquennoy & Mayor 1991), companion stars are usually much less luminous and the resulting shift in the luminosity function is small even at infrared wavelengths. This is true even in the case of pre-main-sequence stars. For example, the mean difference in the K magnitudes of the components of 39 pre-main-sequence binary stars in Taurus and Ophiuchus is $\approx$1.4 mag (Simon *et al.* 1995). This amounts to a typical decrease in the observed magnitude of a YSO binary system (compared to that of the primary alone) of $\Delta m=2.5\ \log(1+10^{-\Delta K/2.5})\approx 0.25$ mag. This is smaller than the bin size used to construct both the model and observed luminosity functions. Consequently, we expect that the shape and structure of the observed and synthetic KLFs are not much altered by the presence of unresolved binary systems since they are only slightly more luminous than single stars.

Second, the presence of unresolved binaries can result in an underestimate of the numbers of the lowest luminosity stars compared to what would be expected for a luminosity function of purely single stars (Kroupa *et al.* 1991). This is simply because the low luminosity companions of brighter primary stars are not detected and thus not counted as separate objects. However, this effect is largely taken into account in our models by virtue of our choice of the field star IMF as the underlying mass function of our synthetic clusters. The adopted field star IMF is derived from the field star luminosity function which is also not a single star luminosity

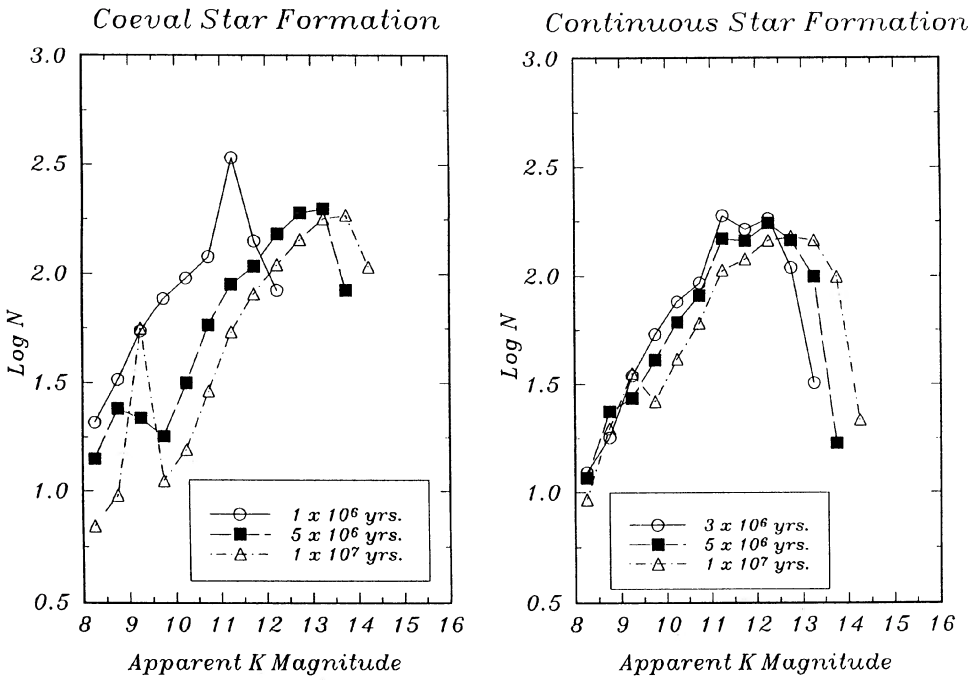

FIG. 5. Model K luminosity functions. (a) The KLF constructed for model clusters assuming coeval star formation. The models are presented for cluster ages equal to 1×10^6, 5×10^6, and 10×10^6 yr old. (b) The KLF models for clusters exhibiting continuous star formation at a constant rate. The continuous star formation models are presented for maximum cluster ages equal to 3×10^6, 5×10^6, 7×10^6, and 10×10^6 yr old. All the models in (a) and (b) have been corrected for the distance modulus of IC 348 ($m-M=7.5$).

function (Kroupa *et al.* 1991). The field star luminosity function is derived from a sample of stars which extends to 100 pc from the sun. At 100 pc the typical binary star has a separation of 0.3 arcsec (Duquennoy & Mayor 1991), much smaller than the 1–3 arcsec resolving power of the observations used to construct the luminosity function. Since the fraction of all stars which are expected to be binaries with separations between 100–800 AU is small (≈10%: Duquennoy & Mayor 1991), the presence or lack of such stellar systems is not likely to be a significant source of uncertainty in the comparison of our single star synthetic KLFs with observations of IC 348 or any other nearby young cluster.

5.2.3 Coeval star formation models

The model KLFs were first obtained for clusters characterized by coeval star formation. In these models stars are assumed to be created in such a manner that they all appear at the birthline in the HR diagram at the same instant in time. Synthetic KLFs were calculated for a set of ten coeval clusters ranging in age from 10^6 to 10^7 yr in 10^6 yr intervals. Representative results of our modeling are presented in Fig. 5(a). This figure plots $\log N$ vs K magnitude, corrected for the IC 348 distance modulus, $m-M=7.5$ (Strom *et al.* 1974) for cluster ages one, five, and ten million years, respectively. Comparison of the model KLFs shows that the shape and extent of the KLF of a coeval cluster change with age. The most noticeable difference is that the 10^6 yr old KLF turns over much earlier and has a much narrower distribution than the models for the older clusters. This can be understood in terms of the luminosity evolution of low PMS mass stars, i.e., as low mass stars approach the main-sequence, their luminosities decrease toward their main-sequence values. For the 10^6 yr old cluster, the model KLF begins to turn over at $m_K=11.0$ and truncates at $m_K\sim12.5$, whereas the 5 and 10×10^6 yr old cluster KLFs turn over a magnitude fainter at $m_K\sim12.5$ and 13.5 and truncate at $m_K\sim13.5$ and 14.5, respectively.

A linear least-squares analysis was performed on the model data over a magnitude range similar to that fit to IC 348 ($m_K<11$). The resulting slopes are summarized in Table 2. As one might expect, the slope determined for the 1×10^6

TABLE 2. Slopes of near-infrared luminosity functions.

Observed Luminosity Funtions	
Cluster	α_K
IC 348	0.40
Trapezium	0.38
NGC 2024	0.37
NGC 2071	0.38
NGC 2068	0.37
NGC 2264	0.32

Model Luminosity Functions		
Cluster Age	α_K	
	Coeval Models	Continuous Models
1×10^6	0.36	–
2×10^6	0.37	0.37
4×10^6	0.31	0.36
6×10^6	0.26	0.37
8×10^6	0.26	0.39
10×10^6	0.27	0.40

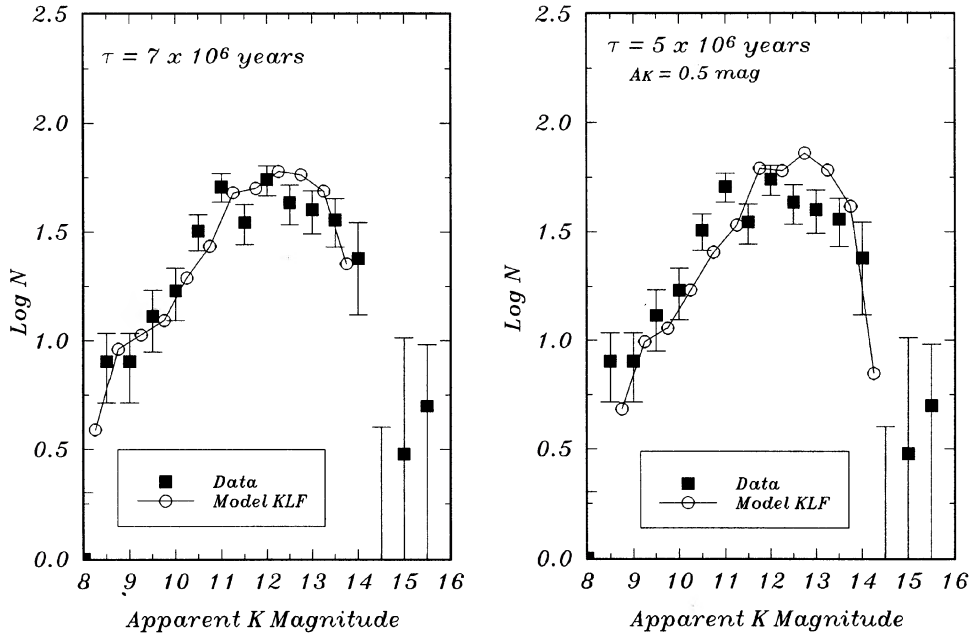

FIG. 6. Comparison of model and IC 348 K luminosity functions. (a) The 7 Myr continuous star formation model KLF with the observed IC 348 KLF. (b) The 5 Myr continuous model corrected for extinction with the IC 348 KLF. Both models have been normalized to provide the best fit to the data over the entire magnitude range above the completeness limits of the observations.

yr old model (0.36) is steeper than the slopes determined for the 5×10^6 and 10×10^6 yr old models (0.24 and 0.27, respectively). However, the significance of this is not clear since the model (coeval) KLFs are not as well characterized by simple power law shapes over the same intervals as the observations.

5.2.4 Continuous star formation models

In order to investigate the effects of noncoeval star formation on the appearance and evolution of the infrared luminosity function of a young cluster, we also constructed model KLFs for clusters in which star formation was assumed to be a continuous process over the lifetime of the cluster. For the continuous star formation models synthetic KLFs were constructed for maximum cluster ages, tmax, ranging from $2–10\times10^6$ yr old in 1×10^6 yr intervals. For each tmax, coeval models, having ages $\leq$tmax, were added together with equal weighting, thus assuming a constant rate of star formation within the cluster. The results for the continuous star formation (CSF) models are presented in Fig. 5(b) for maximum cluster ages, three, five, and ten million years old. The CSF models were also corrected for the distance modulus of IC 348. The overall shapes of the CSF model luminosity functions are similar and do not appear to change significantly with maximum cluster age. However, the extent of the model KLFs do change with age, with the width of the magnitude distribution increasing with increasing age. A linear least-squares analysis was performed on the CSF model data for magnitudes, $m_K<11$. The resulting slopes range from 0.36 to 0.40 and are listed in Table 2. *The slopes of the CSF model luminosity functions are essentially independent of the maximum cluster age* and resemble the slope determined for the 1×10^6 yr old coeval model. Furthermore, these model slopes are remarkably similar to the slopes measured for the K luminosity functions of young embedded clusters (i.e., IC 348, NGC 2264, and the Orion clusters).

5.3 Comparison of Models With Observations

5.3.1 IC 348

The model KLFs were compared to the KLF observed for the IC 348 cluster. None of the coeval models fit the shape of the observed KLF very well between the magnitudes m_K 8–14. The slope of the IC 348 KLF is well matched by the one million year old coeval model. However, this model KLF turns over and truncates several magnitude bins brighter than the observations. In contrast, the older coeval models fit the extent of the observed luminosity function better, but do not fit the slope. The continuous star formation models fit the KLF observed for IC 348 much better than the coeval models do. In particular, the CSF models for cluster ages ranging from $5–10\times10^6$ yr old fit the data reasonably well, with the 7×10^6 yr old model providing the best fit to our data. This is shown in Fig. 6(a) which plots the IC 348 KLF and the 7×10^6 yr old CSF model KLF. Here the model KLF has been normalized to provide the best fit to the data between 8–14 mag. Although the seven million year CSF model can fit the KLF extremely well it may not be appropriate since the cluster appears to suffer extinction (i.e., $A_K\approx0.5$ mags) and this has not been included in the models. To attempt to account for the effects of (uniform) foreground extinction, we extincted our CSF models by 0.5 mag at K

and compared them to the data. The effect of uniform foreground extinction is to introduce a shift in the model KLF toward larger magnitudes (the shape of the KLF is unchanged). Differential extinction could affect the shape of the luminosity function but only if the amount of differential extinction across the cluster significantly exceeds the width of the bins used to construct the luminosity function. This is not a significant problem for the KLF of IC 348. The best fit to the observed data with extincted models was achieved by the five million year CSF model as shown in Fig. 6(b).

Similar evolutionary models for the JLF of a young cluster were also calculated. Comparison of the resulting coeval and CSF models of the JLF with the observed IC 348 JLF yielded results consistent with the results of the KLF modeling. Moreover, we found that to fit the observed data with a 5×10^6 yr CSF model required the extinction at J to be twice as great as that at K just as is expected from the infrared extinction law (i.e., $A_J=2.5A_K$; Rieke & Lebosky 1985). Overall, however, the models (with and without extinction) did not fit the observed JLF as well as the observed KLF. This is likely a result of the fact than the shape of the JLF is considerably more sensitive to the presence of differential extinction than is the KLF. In any event, the above considerations lead us to conclude that the basic properties of the infrared luminosity function of IC 348 are best explained by assuming that (1) the underlying mass function of the cluster is very similar to the field IMF; and (2) that stars have formed in the cluster *continuously* over a period of $5–7\times10^6$ yr.

The concept of a continuous star formation history for IC 348 is not a new one. Additional evidence in support for a long incubation period for the IC 348 cluster comes from the fact that the cluster contains signposts of very recent star formation activity along with a few main-sequence A and B stars. (Herbig 1954; Strom *et al.* 1974). For example, our near infrared observations indicate that sources exhibiting infrared excess emission are found throughout the IC 348 cluster region. Infrared excess emission is common in young stars and arises from the presence of circumstellar material (Rydgren *et al.* 1976; Cohen & Kuhi 1979; Lada & Adams 1992). The amount of the excess is indicative of the nature and distribution of the surrounding material and therefore reveals information about the evolutionary states of the young sources (Lada & Wilking 1984; Adams *et al.* 1987; Myers *et al.* 1987). The near-infrared excesses produced by the excess sources in IC 348 are typical of those of Class II sources in the Taurus and Ophiuchus dark clouds (e.g., Lada & Wilking 1984; Kenyon & Hartmann 1994). In such objects the bulk of the excess emission at two microns wavelength is thought to be produced by the presence circumstellar disks (e.g., Lada & Adams 1992). The lifetime of the disk phase of early stellar evolution is on the order of $\sim3\times10^6$ yr (e.g., Strom *et al.* 1993b) which is shorter than the estimated age of IC 348 ($5–7\times10^6$). The fact that only a small fraction of IC 348 cluster members, ~20%, exhibit near-infrared excess emission therefore supports the idea of a long period of star formation in the cluster. In addition, other indications of recent and ongoing star formation have been observed in this region, such as Herbig's (1954) observation of Hα stars in the cluster and the observation of a molecular hydrogen jet (McCaughrean *et al.* 1994) which is detected in the southwest corner of our K-band image. Although the evidence for recent star formation is robust, the evidence for older stars in the cluster is somewhat less secure. Strom *et al.* (1974) derive an age of $1–2\times10^7$ yr for the cluster by assuming that o Per, which is slightly above the ZAMS, is a cluster member despite its discordant proper motion (Fredrick 1956). There are a few early A (A0–A7) stars appearing on the ZAMS giving a "contraction" age of about 6×10^6 yr for the cluster. At the same time there are two early A stars above the ZAMS, suggesting an age spread of $3–6\times10^6$ yr (Strom *et al.* 1974) consistent with the results of our KLF models. The issue of the age of the cluster is important because if an age of $5–7\times10^6$ yr is established independently of our modeling, then our assumption that the underlying IMF of the cluster is very close to that of field stars would be essentially confirmed.

5.3.2 Uniform rate of star formation?

Although our analysis suggests that star formation was a continuous process in IC 348, it is important to determine if we can place constraints on the extent to which the rate of star formation could have varied with time over the age of the cluster. Our star count maps indicate that the cluster is structured with about half the stars contained in a central subclustering. However, the spatial distribution of near-infrared excess sources, representing one of the youngest components of the cluster population, is more uniform and less subclustered than that of the nonexcess stars. This suggests that star formation has varied in some manner in space or in time within this cluster. Could the large central subcluster have formed in a burst of activity shorter than the five million year time scale of the cluster as a whole? To investigate the possibility of a variable rate of star formation in this cluster we constructed model luminosity functions in which the star formation rate consisted of two components, a burst of duration one million years superposed on an otherwise steady star forming rate. This was accomplished by adding together coeval models with unequal weighting. Specifically for a model cluster age of tmax, the coeval model with age=tmax was given a higher weight than the models with lower ages, which were all given the same lower weight. This allowed us to approximate the case of continuous star formation with a burst of star formation at the time tmax. Four separate "burst" models were constructed for tmax=5, 7, and 10×10^6 yr, respectively. In each case the coeval model with age=tmax was assigned a weight, 30%, 50%, 70%, and 90% higher than the sum of the models with age <tmax, thus representing the case of continuous star formation with a burst of star formation activity at the age tmax, which produces 30%, 50%, 70%, and 90% of the cluster members, respectively. None of the burst models fit the observed data well. The models having a high fraction of stars produced by a burst of star formation ($\geq$50%), have slopes shallower than the observed data, and resemble the coeval model luminosity functions for the respective ages.

These considerations suggest that not only has star formation been a continuous process in IC 348, but that the total

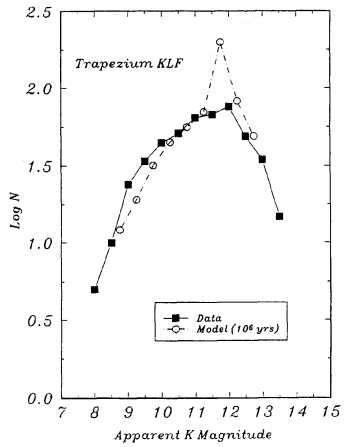

FIG. 7. The KLF for the Trapezium cluster (adapted from Zinnecker *et al.* 1993) is compared to the coeval model KLF for a 1 Myr old cluster. The model KLF assumed a distance modulus to the Trapezium of 8 mag.

star formation rate has been relatively constant over the five–seven million year lifetime of the cluster. Moreover, our CSF modeling implicitly assumes that the star formation rate as a function of mass also does not vary with time. The good agreement of our CSF fits to the data suggest that this is also the case in the cluster. In other words, we find no evidence to indicate that the ratio of low-to-high mass stars being formed changes with time. The star formation rate is a function of mass and that function is essentially independent of time and given by the IMF. The star formation mechanism in this cluster has not produced stars sequentially in mass.

5.3.3 The Trapezium cluster

A prediction of our modeling analysis is that the luminosity function of a young cluster changes it shape in a systematic way as the cluster ages and evolves. In particular, the KLFs of very young clusters will extend over a smaller range of luminosity than those of older clusters and they will be observed to peak at brighter magnitudes than older clusters. Therefore a good test of our evolutionary models would be to see how well they fit clusters of younger ages. Recently Prosser *et al.* (1994) analyzed space telescope observations of the Trapezium cluster and found that the stars in that cluster all had an age $\leq 10^6$ yr. In Fig. 7 we show the KLF of the stars in the central regions of the Trapezium cluster constructed by Zinnecker *et al.* (1993) along with our unextincted 10^6 yr old model KLF corrected for the distance modulus, $m-M=8$ mag, for Orion. The model correctly reproduces the breadth and the location of the peak of the observed KLF and, except for the spike at $K\approx 11$ mag, fits the data extremely well. (The spike in the model KLF is an artifact of the models and results from the inclusion of deuterium burning in the adopted pre-main-sequence tracks coupled with the assumption of coevality. Such a "deuterium burning" spike also appears in the Zinnecker *et al.* (1993) models for clusters with ages less than a million years. The lack of such a peak in the observed luminosity function may be due to the fact that young stellar objects deplete their deuterium supplies in their protostellar stage of evolution before they appear on the HR diagram (Fletcher & Stahler 1994a; Stahler, Shu & Taam 1980). In addition, relaxation of the assumption of coevality would also tend to broaden out this "deuterium peak" and contribute to its absence in the observed data.) Recently, Ali & De Poy (1995) have published a new K-band survey of the Trapezium cluster. Their KLF agrees with that of Zinnecker *et al.* (1993) and their analysis of the KLF also suggests a 10^6 yr age for the cluster if the underlying IMF is similar to the field.

Essentially, with the change of only a single parameter, the cluster age, our models of luminosity function evolution can successfully account for the salient differences between the KLFs of IC 348 and the Trapezium clusters. This serves to reinforce our conclusions that (1) star formation in IC 348 has been a continuous process over the last five to seven million years, a period comparable to the age of the cluster, (2) the rate of star formation has been constant over the lifetime of IC 348 and (3) the underlying IMF of IC 348 (and the Trapezium) is quite similar to that of field stars. Moreover, there appears to be little evidence for a significant population of objects with masses less than the hydrogen burning limit. This latter conclusion is particularly evident from the analysis of the Trapezium cluster where a peak and turnover in the luminosity function are most clearly present and can be accounted for by a model cluster of one million year old stars whose underlying IMF peaks at about 0.2–0.3 $\mathcal{M}_\odot$ and has a low mass cutoff at 0.1 $\mathcal{M}_\odot$, near the hydrogen burning limit. In the earliest stages of evolution low mass pre-main-sequence stars derive their luminosities from loss of gravitational potential energy and deuterium burning. These are the same sources of energy tapped by very young contracting brown dwarf stars (e.g., Burrows *et al.* 1993). Consequently, during these early stages of evolution, the luminosities of brown dwarf stars are considerably closer to those of low mass stars than at later times, especially when stars are able to begin to burn hydrogen on the main sequence. For example, at an age of 3×10^6 yr the ratio of luminosity between a 0.1 $\mathcal{M}_\odot$ star and a 0.05 $\mathcal{M}_\odot$ brown dwarf has a value of only 2.5 (Burrows *et al.* 1993) corresponding to a brightness difference of only 1.0 mag. Thus in young clusters ($\tau_{\rm cl}\leq 10^7$ yr) the more massive brown dwarf stars are not much less luminous than the lowest mass PMS stars and thus brown dwarfs can be readily detected by infrared observations such as those considered here.

5.3.4 Cluster mass and star formation rate

By integrating the model mass function that best fits the data we can determine the total mass of stars contributing to the observed KLF and therefore the total mass of the cluster. In this way we find that the total stellar mass of the IC 348 cluster is 208 ± 20 solar masses for stars in the mass range 0.1–20 solar masses. This is considerably higher than early estimates (~ 40 $\mathcal{M}_\odot$) based on optical observations (Blaauw 1964). The proper motion study of Fredrick (1956) indicates an internal velocity dispersion for the cluster of 1.7 ± 0.8 km s^{-1} which is close to the mean escape velocity for the cluster ($\sqrt{2GM/R}\approx 1.8$ km s^{-1}). This suggests that the

stellar mass of the cluster alone is nearly sufficient to bind the cluster and thus that the star formation efficiency for this cluster is ~50%.

The total star formation rate, estimated over the entire area of the IC 348 cluster, is $\psi = M_{\rm total}/\tau \approx 4\times10^{-5}\ \mathcal{M}_\odot\ {\rm yr}^{-1}$. Similarly, we can derive the star formation rate (SFR) for the Trapezium cluster and we find that rate to be $3\times10^{-4}\ \mathcal{M}_\odot\ {\rm yr}^{-1}$. However, the star formation rate (SFR) we estimate for the Trapezium corresponds to the rate in only a 0.34 pc^{-2} area over which the infrared observations were made (Zinnecker *et al.* 1993). In order to make an appropriate comparison of the SFRs in IC 348 and the Trapezium clusters, it is necessary to determine the rates for both clusters over similar areas. Therefore we also derive a star formation rate for IC 348 in a 0.34 pc^{-2} region and find it to be $1.5\times10^{-5}\mathcal{M}_\odot\ {\rm yr}^{-1}$. Interestingly, the star formation rate in the Trapezium cluster is more than an order of magnitude higher than that in IC 348. Evidently there is a dramatic difference in the physics of the star formation process between the two clusters. Although their underlying mass functions appear to be the same, the process of star formation in the Trapezium cluster has proceeded at a much more rapid pace than that in IC 348. The dramatic difference between the star formation rates in the two clusters suggests that the star formation mechanism in clusters can be very sensitive to initial conditions. Were the masses temperatures, or densities of the dense cores which formed the clusters significantly different? At present it is not clear what property of the parent molecular clouds or general environments of the two regions was responsible for producing such different rates of star formation. One major environmental difference between the two regions is that the Trapezium cluster is associated with a much richer and energetic OB association than IC 348 and one can speculate that the nearby subgroup Ori OB1c could have interacted with the molecular core in which the Trapezium formed, enhancing the star formation rate or even triggering the star formation there (Elmegreen & Lada 1977). However, evolutionary modeling of more clusters needs to be performed to be able to test this or any hypothesis concerning the origin of the large difference in star formation rates observed between these clusters.

5.4 Infrared Excess and Disk Lifetimes

The fraction of infrared excess stars coupled with the age of the cluster can be used to estimate the lifetime of the infrared excess phase and if the excesses are due to circumstellar disks, the lifetime of these disks. Lada & Adams (1992) showed that in Taurus only half of all the stars believed to be Class II sources with disks displayed a large enough excess to be detected in the *JHK* two color diagram. Assuming the same is true for IC 348, we estimate that the total fraction of stars which are Class II sources to be 42%. Thus

$$\tau_{\rm disk} = 0.42\,\tau_{\rm cluster} \approx 2\text{–}3\times10^6\ {\rm yr}.$$

This is consistent with estimates determined from placing Class II sources in the HR diagram (Strom *et al.* 1993b) but should be regarded as a lower limit since it is likely that not all stars began their pre-main-sequence lifetimes with circumstellar disks. In both the Taurus dark clouds and in the Trapezium cluster which have ages of only about one million years, only about half the stars in these regions are Class II sources, suggesting that perhaps only half the stars retain disks by the time they reach the birthline on the HR diagram. If this were the case for IC 348 our estimate of the lifetime of circumstellar disks in the cluster would be increased by a factor of 2.

6. SUMMARY AND CONCLUSIONS

We have obtained sensitive near-infrared imaging observations of the young cluster, IC 348 and have developed models to describe the evolution of the infrared luminosity functions of young embedded clusters of pre-main-sequence stars for comparison with observations. The primary results of our combined study can be summarized as follows.

From comparison of our *JHK* infrared observations of the IC 348 cluster with those of a nearby control field off the cluster we estimate that the cluster population consists of ~380 stars, a substantial increase over previous estimates derived from optical observations. The surface density distribution of these stars is centrally concentrated and decreases inversely with distance from the innermost to the outer most regions of the cluster field. In addition, we find that the spatial distribution of stars exhibits considerable substructure with ~50% of the cluster members contained in a central subcluster 0.5 pc in radius. This central subcluster is surrounded by eight smaller subclusters which typically contain 5–20 stars and have radii between 0.1–0.2 pc. The overall stellar density within the half-mass radius of IC 348 is roughly 220 $\mathcal{M}_\odot\ pc^{-3}$ and is considerably higher than that (2 $\mathcal{M}_\odot\ pc^{-3}$) typical of classical open clusters like the Pleaides. However, the surface densities of the IC 348 cluster and its subclusters range from 70–270 pc^{-2} and are similar to the surface densities of other rich embedded clusters. Analysis of the *JHK* colors reveals that ~20% of the cluster sources are infrared excess sources, suggesting the presence of disks around these young stars. The size of the population of infrared excess sources coupled with the age of the cluster suggests a lifetime of $2\text{–}3\times10^6$ yr for the infrared excess phase or the (protoplanetary) disk phase of early stellar evolution, consistent with previous estimates. We find the *K* luminosity function of IC 348 to increase with magnitude in a nonlinear, power-law fashion in the range $8 \leq m_K \leq 11$ mag. The measured slope (0.40) of the power-law portion of IC 348 KLF is very similar to the slopes (0.37–0.38) determined for the KLFs of four young embedded clusters in Orion. The IC 348 KLF departs from a power-law shape at $m_K > 11$ mag, and appears to decrease at magnitudes ($m_K \approx 14$) near the completeness limit of the survey.

From our modeling of KLF evolution we find that the KLFs of young clusters evolve in a systematic and predictable manner as the clusters age. For clusters in which star formation proceeds at a uniform continuous rate over their lifetimes, the slopes of the power-law portions of their KLFs are found to remain roughly constant for cluster ages of one to ten million years while, the brightness at which the lumi-

nosity functions peak and deviate from a power-law shape, decreases with time producing luminosity functions which broaden with age. The infrared luminosity functions of young clusters in which star formation occurs on a time scale shorter than their age, also broaden with time, however, for these clusters the slopes of the power-law portions of their infrared luminosity functions significantly change with time. The observed similarity of the slopes of the KLFs of numerous young clusters suggests that star formation in many clusters may generally occur in a continuous uniform fashion over the first ten million years of cluster evolution.

Comparison of our infrared observations of IC 348 with the evolutionary models for the KLF has resulted in the conclusions that (1) star formation in IC 348 has been proceeding in a continuous fashion over the last five to seven million years, and (2) that the rate of star formation has been essentially uniform over this entire period. Moreover, no indication exists for a time variation in relative rates at which stars of different mass form. The stellar mass of IC 348 is estimated to be $\sim 200\ \mathcal{M}_{\odot}$ which is nearly sufficient to bind the cluster suggesting that a star formation efficiency of $\sim 50\%$ characterizes this embedded group. A similar analysis of published observations of the Trapezium cluster gives a star formation rate which is at least a factor of 20 times higher than IC 348. These results imply that significant differences exist in at least some of the fundamental details of the star formation process between rich young clusters. On the other hand, comparisons of the model KLFs with the observed KLFs of IC 348 and the Trapezium suggests that the underlying IMFs are the same for both clusters and indistinguishable from the IMF of field stars in the local neighborhood of the Sun. In addition, there appears to be no evidence for a significant population of objects with masses below the hydrogen burning limit.

We thank the KPNO staff for observing and data reduction support, especially Mike Merrill for useful discussions concerning SQIID reduction. We thank Scott Kenyon and Mark Giroux for helpful discussions and input about model luminosity functions. In particular we thank Scott Kenyon for assistance in compiling the m_K–mass relations for late type stars. We thank Hans Zinnecker, John Stauffer, and the referee for helpful comments on our manuscript. Finally we thank Robert Gruendl for assistance in preparing the K-band image of IC 348 for publication. This work was supported in part by NSF Grant No. AST-9314847 and a Hubble Fellowship through Grant No. HF-1047.0193A from STScI to the University of Maryland.

REFERENCES

Adams, F. C., Lada, C. J., & Shu, F. H. 1987, ApJ, 321, 788
Ali, B. & De Poy, D. 1995, AJ, 109, 709
Bachiller, R., Guilloteau, S., & Kahane, C. 1987, A&A, 173, 324
Bachiller, R., & Cernicharo, J. 1986, A&A, 166, 283
Barsony, M., Schombert, J. M., & Kis-Halas, K. 1991, ApJ, 379, 221
Blaauw, A. 1964, ARA&A, 2, 213
Burrows, A., Hubbard, W. B. Saumon, D., & Lunine, J. L. 1993, ApJ, 406, 158
Carpenter, J. M., Snell, R. L., Schloerb, P. F., & Strutskie, M. F. 1993, ApJ, 407, 657
Cohen, M., & Kuhi, L. V. 1979, ApJS, 41, 743
D'Antonna, F., & Mazitelli, I. 1994, ApJS, 90, 467
Duquennoy, A., & Mayor, M. 1991, A&A, 248, 485
Eiroa, C., & Casali, M. M. 1992, A&A, 262, 468
Elmegreen B. G., & Lada, C. J. 1977, ApJ, 214, 725
Fletcher, A. B., & Stahler, S. W. 1994a, ApJ, 435, 313
Fletcher, A. B., & Stahler, S. W. 1994b, ApJ, 435, 329
Fredrick, L. W. 1956, AJ, 61, 437
Gomez, M., Hartmann, L., Kenyon, S. L., & Hewitt, R. 1993, AJ, 105, 1927
Herbig, G. H. 1954, PASP, 66, 19
Hodapp, K. W., & Rayner, J. T. 1991, AJ, 102, 1108
Kenyon, S., & Hartmann, L. 1994, AJ (in press)
Kroupa, P., Tout, C. A., & Gilmore, G. 1991, MNRAS, 251, 292
Kutner, M. L., Machnik, D. E., Tucker, K. D., & Dickman, R. L. 1980, ApJ, 237, 734
Lada, C. J., Margulis, M., & Dearborn, D. 1984, ApJ, 285, 141
Lada, C. J., & Wilking, B. A. 1984, ApJ, 287, 610
Lada, C. J., & Lada, E. A. 1991, ASP Conf. Ser. 13, The Formation and Evolution of Star Clusters, edited by K. Janes (ASP, San Francisco), p. 3
Lada, C. J., DePoy, D., Merrill, M., & Gatley, I. 1991a, ApJ, 374, 533
Lada, E. A., DePoy, D. L. , Evans, N. J., & Gatley, I. 1991b, ApJ, 371, 171
Lada, C. J., & Adams, F. C. 1992, ApJ, 393, 278
Lada, C. J., Young, E. T., & Greene, T. P. 1993, ApJ, 408, 471
Lada, C. J. 1994, in The Cold Universe, edited by T. Montmerle, C. J. Lada, F. Mirabel, and J. T. T. Van (Reidel, Dordrecht), p. 211
Lada, E. A., Evans, N. J., & Falgarone, E. 1995, ApJ, in preparation
McCaughren, M. J., & Stauffer, J. R. 1994, AJ (submitted)
McCaughren, M. J., Rayner, J. T., & Zinnecker, H. 1994, ApJ, 436, L189
Merrill, M. 1992, private communication
Miller, G. E., & Scalo, J. M. 1979, ApJS, 41, 513
Myers, P. C., Fuller, G. A., Mathieu, R. D., Beichman, C. A., Benson, P. J., Schild, R. E., & Emerson, J. P. 1987, ApJ, 319, 340
Patel, K., & Pudritz, R. 1994, ApJ (in press)
Prosser, C. F., Stauffer, J. R., Hartmann, L., Soderblom, D. R. Jones, B. F., Werner, M. W., & McCaughren, M. J. 1994, ApJ, 421, 517
Reid, N. 1993, MNRAS, 265, 785
Rieke, G. H., & Lebosky, M. 1985, ApJ, 288, 618
Rydgren, A. E., Strom, S. E., & Strom, K. M. 1976, ApJS, 30, 307
Salpeter, E. E. 1955, ApJ, 121, 161
Scalo, J. M. 1978, in Protostars and Planets, edited by T. Gehrels (University of Arizona Press, Tucson), p. 265
Scalo, J. M. 1986, Fund. Cosmic Phys. 11, 1
Simon, M., Chen, W. P., Howell, R. R., Benson, J. A., & Slowik, D. 1992, ApJ, 384, 212
Simon, M., *et al.* 1995, ApJ (in press)
Stahler, S. W., Shu, F. H., & Taam, R. E. 1980, ApJ, 241, 637
Stauffer, J. R., Hamilton, D., Probst, R., Rieke, G., & Mateo, M. 1989, ApJ, 344, L21
Stetson, P. 1987, PASP, 99, 191
Straw, S. M., & Hyland, A. R. 1989, ApJ, 340, 318
Strom, S. E., Strom, K. M., & Carrasco, L. 1974, PASP, 86, 798
Strom, K. M., Strom, S. E., & Merrill, K. M. 1993a, ApJ, 412, 233
Strom, S. E., Edwards, S., & Strutskie, M. 1993b, in Protostars and Planets III, edited by E. H. Levy, J. I. Lunine, and M. S. Mathews (University of Arizona Press, Tucson), p. 837
Taff, L. G. 1974, AJ, 79, 1280
Witt, A. N., & Schild, R. E. 1986, ApJS, 62, 839
Zinnecker, H., McCaughrean, M. J., & Wilking, B. A. 1993, in Protostars and Planets III, edited by E. H. Levy, J. I. Lunine, and M. S. Mathews (University of Arizona Press, Tucson), p. 429

FIG. 1. The distribution of 2.2 μm sources toward the young cluster, IC 348. This *K*-band image is a mosaic of 24 individual SQIID images and covers a total area of approximately 385 square arcmin.

E. A. Lada and C. J. Lada (see page 1685)

